Nanoscale

RSC Publishing

PAPER

View Article Online
View Journal | View Issue

Cite this: *Nanoscale*, 2013, **5**, 6908

Precisely controlled resorcinol–formaldehyde resin coating for fabricating core–shell, hollow, and yolk–shell carbon nanostructures†

Xiaoliang Fang,*[ab] Shengjie Liu,[bc] Jun Zang,[d] Chaofa Xu,[b] Ming-Sen Zheng,[d] Quan-Feng Dong,[d] Daohua Sun[c] and Nanfeng Zheng*[b]

Received 6th April 2013
Accepted 19th May 2013

DOI: 10.1039/c3nr01723k

www.rsc.org/nanoscale

This work provides a facile one-step sol–gel route to synthesize high-quality resorcinol–formaldehyde (RF) resin coated nanocomposites that can be further used to fabricate desired carbon nanostructures. Colloidal particles with different morphologies and sizes can be coated with high-quality RF resin shells by the proposed cationic surfactant assisted RF resin coating strategy. The as-synthesized RF resin coated nanocomposites are ideal candidates for selective synthesis of core–shell, hollow, and yolk–shell carbon nanostructures. Based on the carboxylic functional RF resin coating, graphitic carbon nanostructures can also be synthesized by employing the graphitization catalyst. The as-synthesized carbon nanostructures show the advantageous performances in several applications. Hollow carbon spheres are potential electrode materials for lithium–sulfur batteries. Hollow graphitic spheres are promising catalyst supports for oxygen reduction reaction. And yolk–shell structured Au@HCS nanoreactors with ultrathin shells exhibit high catalytic activity and recyclability in confined catalysis.

Introduction

Hollow and core–shell structured nanomaterials have been intensively investigated over the past decade.[1–8] Among these materials, hollow and core–shell nanostructures with carbon shells have attracted considerable attention in catalysis,[9–12] lithium-ion batteries,[13–17] fuel cells,[18] supercapacitor electrodes,[19] adsorption,[20] and photothermal therapy[21] because of the unique properties of carbon shells, such as high specific surface area, large pore volume, high structural and mechanical stability, and good electrical conductivity. As a hybrid of hollow and core–shell carbon nanostructures, the interior of hollow carbon nanostructures decorated by encapsulating functional nanoparticles, which is known as yolk–shell carbon nanostructures, is especially beneficial for catalytic applications.[22–26] The yolk–shell carbon nanostructures with noble metal cores have been applied as stable nanoreactors for confined catalysis and they have shown excellent catalytic performance in catalytic hydrogenation reactions.[22–26] In previous studies, the hard-templating method is a very effective strategy for selective synthesis of core–shell, hollow, and yolk–shell carbon nanostructures.[22–26] An apparent advantage of the hard-templating method is that the structure parameters (*e.g.*, shape and size) of the as-synthesized core–shell, hollow, and yolk–shell carbon nanostructures can be easily and precisely controlled by the pre-fabricated templates.[27] In a typical hard-templating approach, the template is first coated with a layer of carbon precursors followed by carbonization, yielding core–shell carbon nanostructures. After removal of the templates, the core–shell carbon structures can be further converted into hollow carbon nanostructures.[9–11] Following similar procedures, when employing the silica coated composites as the templates, yolk–shell carbon nanostructures can be obtained after the selective removal of the silica layer in the sandwich-like core@silica@carbon nanostructures.[22–26] The coating of the pre-fabricated templates with appropriate carbon precursors is thus an important process for selective synthesis of the core–shell, hollow, and yolk–shell carbon nanostructures.

[a]*Pen-Tung Sah Institute of Micro-Nano Science and Technology, Xiamen University, Xiamen 361005, China. E-mail: x.l.fang@xmu.edu.cn*

[b]*State Key Laboratory for Physical Chemistry of Solid Surfaces, Collaborative Innovation Center of Chemistry for Energy Materials, Department of Chemistry, Xiamen University, Xiamen 361005, China. E-mail: nfzheng@xmu.edu.cn*

[c]*Department of Chemical Engineering, Xiamen University, Xiamen 361005, China*

[d]*Department of Chemistry, Xiamen University, Xiamen 361005, China*

† Electronic supplementary information (ESI) available: Synthesis of ellipsoid-shaped α-Fe_2O_3@SiO_2 core–shell nanoparticles; preparation of HCS-260/sulfur composites; electrochemical measurement of lithium–sulfur batteries; SEM image of SiO_2@RF spheres; TEM image of SiO_2@RF spheres obtained by using cetyltrimethylammonium chloride; TEM images of SiO_2@RF spheres with different diameters of SiO_2 cores; TEM images for investigating the roles of CTAB; N_2 sorption isotherms and pore size distributions of HCS-260 and HGS-260; TEM image and EDX spectrum of HCS-260/sulfur composites; cycling performance of lithium–sulfur batteries with HCS-260/sulfur cathode; HRTEM image of HGS-260; XRD patterns of Pt/HGS, Pt/HCS, and Pt/Vulcan-XC-72; TEM image of Au@SiO_2 UV-vis spectra of the gradual reduction of 4-nitrophenol with Au@HCS-II, Au@HCS-III, and Au@HCS-IV. See DOI: 10.1039/c3nr01723k

It is well known that carbon precursors play an important or even decisive role in the final physical and chemical properties of the resulting carbon framework.[28] Many carbon precursors, such as resorcinol–formaldehyde (RF) resin, saccharide, pitch, and polydopamine, have been used to fabricate carbon nanostructures.[29–36] Among these carbon precursors, RF resin, a three-dimensional network structured polymer, is highly fascinating due to the attractive properties of RF resin derived carbon such as low cost, high surface areas, high porosities, controllable pore structures, low electrical resistivity, remarkable electrical conductivity, and outstanding thermal and mechanical properties.[37,38] Over the past two decades, RF resin has been widely applied to the fabrication of various carbon nanomaterials, such as carbon aerogels and xerogels,[37,38] ordered mesoporous carbon,[39–41] and colloidal carbon spheres.[42,43] Due to the lack of an effective route to obtain high-quality RF resin coated core–shell nanostructures, the impregnation of the prefabricated RF resin into core–shell structured mesoporous silica is a prevalent route to synthesize RF resin derived hollow and yolk–shell carbon nanostructures although the multi-step procedures are inevitable.[22–26] From the viewpoint of fundamental research, it is still desirable to develop a straightforward and general route to manipulate RF resin coating for selective synthesis of the core–shell, hollow, and yolk–shell carbon nanostructures. It is noteworthy that the structure parameters of carbon nanostructures play critical roles in their targeted applications. In some catalytic applications, hollow carbon nanostructures with graphitic shells are highly desired.[9–11] Since the carbon materials obtained by direct carbonization of RF resin are usually non-graphitizable,[28] the RF resin coating for synthesis of hollow carbon nanostructures with graphitic shells is still faced with challenges. When yolk–shell carbon nanostructures are used as the carbon nanoreactors, the ultrathin carbon shells are beneficial to their catalytic performance due to facile diffusion of the reaction substances.[36] Consequently, the controllable RF resin coating for synthesis of yolk–shell carbon nanostructures with ultrathin shells would open new opportunities for high-performance carbon nanoreactors.

Herein, we report a facile hard-templating route to synthesize high-quality RF resin coated nanocomposites based on a one-step sol–gel polymerization of resorcinol and formaldehyde in the presence of cationic surfactant cetyltrimethylammonium bromide (CTAB). By investigating the roles of CTAB, we revealed the importance of CTAB in promoting polymerization of resorcinol and formaldehyde at low concentrations. Since the highly controllable RF resin coating process developed in this work is applicable to various template materials, the proposed synthetic strategy provides an ideal platform for the design and synthesis of core–shell, hollow, and yolk–shell nanostructures. Moreover, a functional group modified RF resin coating process is proposed as an improved synthetic strategy to further fabricate hollow carbon nanostructures with graphitic shells. By choosing SiO_2 spheres and SiO_2 coated composites as templates, we successfully synthesized hollow carbon spheres (HCS), hollow graphitic spheres (HGS), and yolk–shell carbon nanostructures with ultrathin shells. For applications, we demonstrate that the as-synthesized HCS are potential electrode materials for lithium–sulfur batteries. The obtained HGS are promising catalytic supports for oxygen reduction reaction (ORR), and the prepared yolk–shell carbon nanostructures with ultrathin shells are ideal nanoreactors for confined catalysis.

Experimental

Chemicals

Tetraethyl orthosilicate (TEOS), resorcinol, potassium hexachloroplatinate(IV) and 2,4-dihydroxybenzoic acid were purchased from Alfa Aesar; ammonia solution (25–28%), cetyltrimethylammonium bromide, ethanol, formaldehyde, $HAuCl_4 \cdot 3H_2O$, sodium citrate and $FeCl_3 \cdot 6H_2O$ were purchased from Sinopharm Chemical Reagent Co. (Shanghai, China). All the reagents were used without further purification. Deionized water was used in all experiments.

Synthesis of SiO_2 spheres, α-Fe_2O_3 spindles, and Au@SiO_2

SiO_2 spheres were synthesized following a slightly modified Stöber process. In a typical synthesis, 6 mL of TEOS was rapidly added into a mixture of 75 mL of ethanol, 10 mL of deionized water, and 3.15 mL of ammonium aqueous solution, and then stirred at room temperature for 1 h. The SiO_2 spheres were centrifugally separated from the suspension and washed with deionized water and ethanol. The α-Fe_2O_3 spindles were synthesized by aging a solution containing 136 mg of $FeCl_3 \cdot 6H_2O$, and 2 mg of NaH_2PO_4 dissolved in 16 mL of deionized water at 180 °C for 6 h. Core–shell structured Au@SiO_2 was synthesized as follows. 18.0 mg of $HAuCl_4 \cdot 3H_2O$ was dissolved in 30 mL water and heated to boil under vigorous stirring. 1.0 mL (3.0 wt%) of sodium citrate aqueous solution was injected quickly into the above mixture and then refluxed for 30 min. After the solution was cooled down to room temperature, an aqueous solution of 0.235 mL of PVP 10 (12.8 g L^{-1}) was added to the colloidal gold solution to modify the surface of Au nanoparticles to facilitate silica coating. The solution was stirred for 24 h at room temperature. The PVP-modified gold nanoparticles were collected by centrifugation and re-dispersed in 2.0 mL water. For silica coating, 1.0 mL of gold nanoparticles covered by PVP was added into a mixture of 46 mL of isopropanol, 6.6 mL of H_2O, and 1.28 mL of ammonium. Then 0.4 mL of TEOS was added under vigorous stirring and stirring was continued for another 6 h. The Au@SiO_2 was collected by centrifugation and then washed with deionized water and ethanol.

RF resin coating

The as-prepared SiO_2 spheres were homogeneously dispersed in the mixture of deionized water and ethanol by ultrasonication, followed by the addition of CTAB, and then stirring at room temperature. The mixed solution was homogenized for 20 min to form a uniform dispersion. Resorcinol and formaldehyde were added to the dispersion with continuous stirring for 10 min. After the addition of ammonia solution, the weight ratio of SiO_2–CTAB–resorcinol–formaldehyde–H_2O–ethanol–ammonia solution was 1 : 1.5 : 0.32 : 0.49 : 600 : 197 : 3.64. The final

mixture was stirred at room temperature (25 °C) for 20 h, and the products, SiO_2@RF core–shell spheres, were collected by centrifugation. The RF resin coating procedures for SiO_2 can be directly applied to other colloids, resulting in the formation of numerous core–shell structured RF resin coated nanocomposites. Under the same reaction conditions for synthesis of SiO_2@RF core–shell spheres, the weight ratios of Au@SiO_2–resorcinol–formaldehyde used in the synthesis of Au@SiO_2@RF-I, -II, -III, and -IV are 1/0.08/0.13, 1/0.16/0.25, 1/0.32/0.49, 1/0.64/0.98, respectively.

Versatile carbon nanostructures

The core–shell carbon nanostructures were obtained by the carbonization of core–shell structured RF resin nanocomposites under a N_2 atmosphere at 350 °C for 2 h with a heating rate of 1 °C min^{-1}, which was followed by further treatment at 800 °C for 4 h with a heating rate of 1 °C min^{-1}. After washing with 2 M NaOH aqueous solution for 24 h, the as-synthesized SiO_2@C, Au@SiO_2@C, and Fe_3O_4@SiO_2@C were converted into HCS, Au@HCS, and Fe_3O_4@HCS, respectively.

Hollow graphitic spheres

Carboxylic functional RF resin coating of SiO_2 composites was synthesized under similar reaction conditions for the above RF resin coating of SiO_2 spheres except replacing resorcinol with the mixture of resorcinol and 2,4-dihydroxybenzoic acid, and the final weight ratio of SiO_2–CTAB–resorcinol–2,4-dihydroxybenzoic acid–formaldehyde–H_2O–ethanol–ammonia solution was 1 : 1.5 : 0.32 : 0.1 : 0.49 : 600 : 197 : 3.64. The as-synthesized SiO_2@RF–COOH was first immersed in 0.25 M $FeCl_3 \cdot 6H_2O$ aqueous solution overnight to load the graphitization catalyst, and then washed with deionized water and ethanol, dried at 60 °C for 4 h. After carbonizing at 800 °C under a N_2 atmosphere for 4 h, the SiO_2@graphitic shell was obtained. Subsequently, the obtained SiO_2@graphitic shell was treated with concentrated HCl (37%) for 10 h and 2 M NaOH aqueous solution for 24 h. Finally, the hollow graphitic spheres were obtained by centrifugation and washed with water and ethanol.

Synthesis of Pt/HGS, Pt/HCS, and Pt/Vulcan-XC-72

The carbon supports (*i.e.*, HGS-260, HCS-260, and Vulcan-XC-72 carbon) were first treated with 30% nitric acid aqueous solution at 100 °C for 5 h, and then washed with deionized water until the pH values of the wash solution was in the near-neutral range, and dried at 60 °C for 6 h. Subsequently, 10 mL of ethylene glycol and 8.0 mg of potassium hexachloroplatinate(IV) were mixed in a 50 mL flask with continuous stirring at 60 °C for 1 h, and followed by the addition of 40 mg of acid treated carbon supports. The mixture was heated to 60 °C and held for 1 h with continuous stirring. After cooling to room temperature, the products were collected by centrifugation and washed with ethanol.

Electrochemical studies

0.05 mg Pt-containing catalysts (based on the inductively coupled plasma-atomic emission spectroscopy measurements) were dispersed in 1 mL of ethanol, and then ultrasonicated to form uniform black ink. The catalyst modified RDE was prepared by applying 60 μL well-dispersed catalyst ink onto the pre-polished RDE. Therefore, the Pt loading was 15.3 μg cm^{-2}. After drying at room temperature, 5 μL of 0.1 wt% Nafion solution was applied onto the surface of the catalyst layer to form a layer protecting catalyst particles from detaching. Prior to electrochemical experiments, the catalyst modified RDEs were subjected to continuous potential cycling (0 to 1.1 V *vs.* RHE, 50 mV s^{-1}) in 0.1 M aqueous $HClO_4$ until cyclic voltammograms became reproducible. The ORR measurements were performed in 0.1 M $HClO_4$ solutions under flow of O_2 using the catalyst modified RDE at a rotation rate of 1600 rpm and a sweep rate of 10 mV s^{-1}. In the ORR polarization curve, current densities (j) were normalized in reference to the geometric area of the glassy carbon RDE (0.196 cm^2). For the ORR at a RDE, the kinetic current (j_k) was calculated based on the Koutecky–Levich equation:

$$\frac{1}{j} = \frac{1}{j_k} + \frac{1}{j_d}$$

where j is the experimentally measured current, j_d is the diffusion-limiting current, and j_k is the kinetic current.

Catalytic reduction of 4-nitrophenol with Au@HCS

Au@HCS with 3×10^{-4} mmol of Au cores was homogeneously dispersed in 5 mL of deionized water by ultrasonication, followed by the addition of 0.5 mL of $NaBH_4$ aqueous solution (0.5 M), and the mixture was stirred for 10 min at room temperature. 0.25 mL of 4-nitrophenol (0.12 M) was then added to the mixture, which was stirred until the deep yellow solution became colorless. During the course of reaction, the reaction progress was monitored by measuring UV-vis absorption spectra of the mixture.

Characterization

Scanning electron microscopy (SEM) and transmission electron microscopy (TEM) images were taken on a Hitachi S-4800 microscope with a field-emission electron gun and a TECNAI F-30 high-resolution transmission electron microscope operating at 300 kV, respectively. The phase of the products was characterized by X-ray powder diffraction (XRD, Panalytical X'pert PRO diffractometer with Cu-Kα radiation). The surface area of the as-synthesized carbon nanostructures was measured by the Brunauer–Emmett–Teller (BET) method using nitrogen adsorption and desorption isotherms on a Micrometrics ASAP 2020 system. The pore size distribution plot was obtained by the Barrett–Joyner–Halenda (BJH) method. The UV-vis spectra were recorded in the range of 210–800 nm with a Varian Cary 5000 spectrometer.

Results and discussion

Cationic surfactant assisted RF resin coating strategy

The procedure for selective synthesis of core–shell, hollow, and yolk–shell carbon nanostructures is shown in Scheme 1. The

target core materials (*e.g.*, colloid particles or silica coated composites), resorcinol, and formaldehyde were first mixed in a mixture of H_2O, alcohol, ammonia, and CTAB. The RF resin coated core–shell nanostructures were obtained at room temperature by a facile one-pot sol–gel process involving base catalytic co-assembly of resorcinol/formaldehyde/CTAB and deposition of RF resin onto the surface of target core materials. From the RF resin coated nanocomposites, core–shell carbon nanostructures were directly synthesized by carbonization. Hollow or yolk–shell carbon nanostructures were further obtained by the selective etching of the template layers.

Fig. 1 shows SEM and TEM images of the SiO_2@RF core–shell spheres synthesized by using SiO_2 spheres with a particle size of *ca.* 260 nm (designated as SiO_2-260) as the templates (Fig. 1a). It is apparent that highly uniform and monodisperse RF resin coated nanocomposites are obtained, and each SiO_2@RF core–shell sphere contains only one SiO_2 core at the center (Fig. 1b and c and S1†). Similar SiO_2@RF core–shell spheres can be synthesized by using other cationic surfactants (Fig. S2†). The synthetic approach is highly reproducible and scalable, and 5 g of SiO_2@RF core–shell spheres could be easily prepared in a one-pot reaction. After the removal of CTAB by the extraction of SiO_2@RF core–shell spheres with the mixture of hydrochloric acid and ethanol,[44] the yield of the RF shells is approximately 85% evaluated from the weight of the reactants resorcinol and formaldehyde. It is worth noting that the structure parameters of the as-synthesized SiO_2@RF core–shell spheres are highly controllable. As a primary advantage of the developed synthetic approach, the thickness of RF resin shells could be precisely tailored from 40 nm to 3 nm by reducing the amount of resorcinol and formaldehyde whilst keeping the other synthetic parameters constant (Fig. 1d–g). Furthermore, the size of SiO_2@RF core–shell spheres could be tunable by varying the size of templating SiO_2 spheres (Fig. 1h and i and S3†).

The roles of the cationic surfactant were found to be very critical in the developed RF resin coating process. Recently, Lu and co-workers have demonstrated that RF resin spheres can be synthesized by the polymerization of resorcinol (~7.14 mg mL^{-1}) and formaldehyde (~11.0 mg mL^{-1}) in a mixture of H_2O–alcohol–ammonia.[42] Therefore, we tried to synthesize SiO_2@RF core–shell spheres under the same synthetic conditions but in the absence of CTAB (Fig. 2a). Unfortunately, due to the low concentration of resorcinol (≤0.38 mg mL^{-1}) and formaldehyde (≤0.58 mg mL^{-1}) used for RF coating, no core–shell structures were obtained after the reaction. Only the original SiO_2 spheres were observed (Fig. 2b). To investigate the roles of CTAB, control experiments were designed to simplify the reaction system. As shown in Fig. 2a, no collectable solid RF resin products were obtained if only polymerization of resorcinol (~0.38 mg mL^{-1}) and formaldehyde (~0.58 mg mL^{-1}) occurred in the mixture of H_2O–alcohol–ammonia. Interestingly, when CTAB was added into the same reaction mixture, the spherical RF resin colloids were yielded (Fig. 2a and c). Furthermore, hydrothermal polymerization of phenol and hexamethylenetetramine in the water is a recently arisen method for the encapsulation of polystyrene spheres (PS) with RF resin.[27] We have also used this method to synthesize SiO_2@RF core–shell spheres. As shown in Fig. 2d and S4,† only RF resin spheres and etched SiO_2 spheres can be observed after hydrothermal reaction using the literature method.[27] It is well-known that the co-assembly of resorcinol, formaldehyde, and CTAB in the alkaline solution can form solid RF particles or wires.[44] Based on the good affinity of CTAB with the SiO_2 spheres under the alkaline conditions,[7] CTAB should at least play the following two important roles in the developed method reported here: (1) to promote polymerization of resorcinol and formaldehyde at low concentrations and (2) to induce spontaneous deposition of RF resin onto the surface of silica spheres.

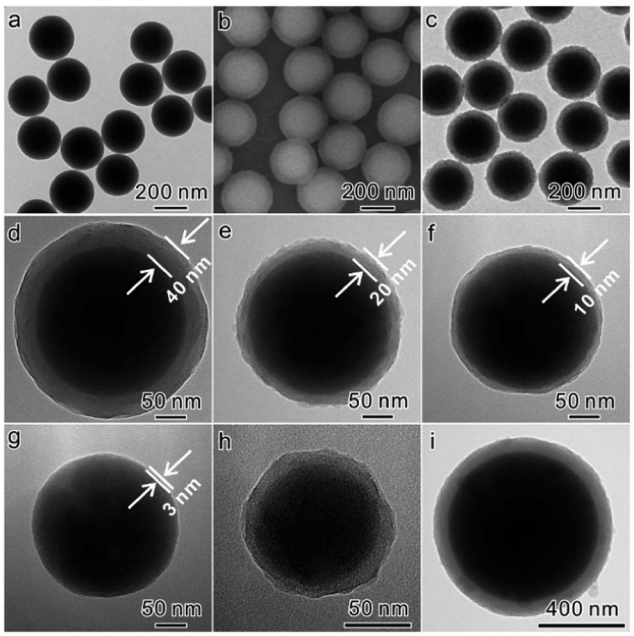

Fig. 1 (a) TEM image of SiO_2 spheres; (b) SEM image and (c) TEM image of SiO_2@RF core–shell spheres; typical TEM images of SiO_2@RF core–shell spheres with different thicknesses of shells: (d) 40 nm, (e) 20 nm, (f) 10 nm and (g) 3 nm; typical TEM images of SiO_2@RF core–shell spheres with different diameters of SiO_2 cores: (h) 100 nm and (i) 750 nm.

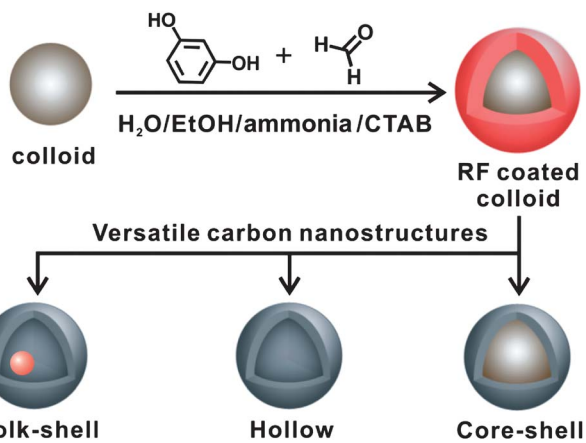

Scheme 1 Schematic illustration of selective synthesis of core–shell, hollow, and yolk–shell carbon nanostructures by the cationic surfactant assisted RF resin coating strategy.

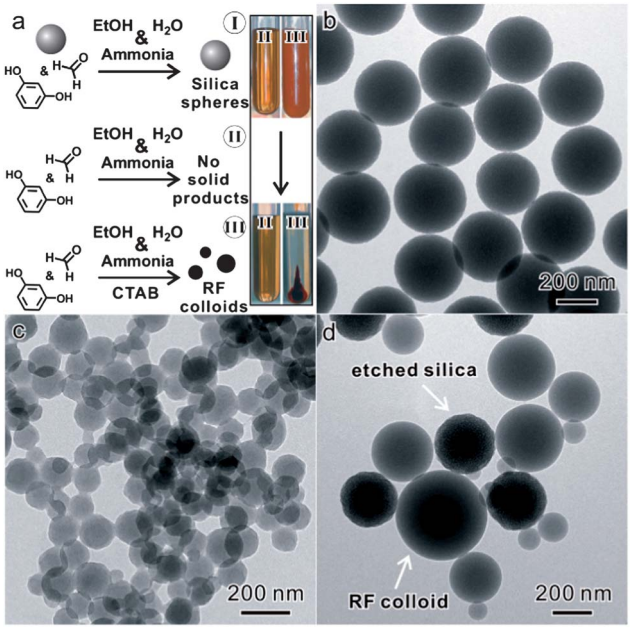

Fig. 2 (a) Scheme of the control experiments; inset photos: the reaction solution of the control experiments II and III before and after centrifugation; (b–d) TEM images: (b) silica spheres obtained by control experiment I and (c) solid RF colloids obtained by control experiment III; (d) the products obtained by hydrothermal reaction of phenol and hexamethylenetetramine in the presence of SiO_2 spheres.

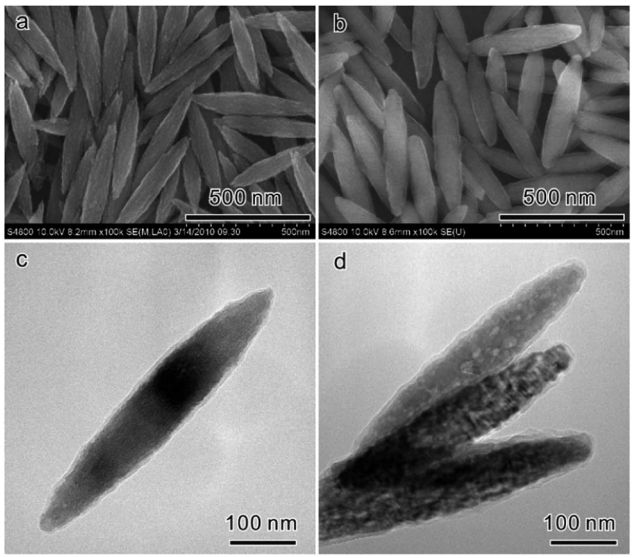

Fig. 3 (a) SEM image of ellipsoid-shaped α-Fe_2O_3 nanoparticles; (b) SEM image and (c) typical TEM image of ellipsoid-shaped α-Fe_2O_3@RF core–shell nanoparticles; (d) typical TEM image of ellipsoid-shaped Fe_3O_4@C core–shell nanoparticles.

Carbon coated core–shell nanostructures

Considering that CTAB has good affinity with a variety of colloidal particles in the mixture of H_2O–alcohol–ammonia,[45–47] we explored the possibility of using our method to synthesize other RF resin coated nanocomposites. To demonstrate the effectiveness of the method to encapsulate non-spherical nanoparticles with RF resin shells, ellipsoid-shaped α-Fe_2O_3 nanoparticles (Fig. 3a) were prepared. As illustrated in Fig. 3b and c, ellipsoid-shaped α-Fe_2O_3@RF core–shell nanoparticles were successfully obtained. After the carbonization under the N_2 atmosphere, α-Fe_2O_3@RF core–shell nanoparticles were converted into Fe_3O_4@C core–shell nanoparticles (Fig. 3d), which have been demonstrated as a promising electrode material for lithium-ion batteries.[13] In addition, we have also successfully synthesized SnO_2@RF, TiO_2@RF, and PS@RF core–shell nanocomposites by the developed synthetic approach. We thus believe that the RF resin coating strategy developed in this work is applicable to the synthesis of carbon coated core–shell nanostructures with a wide range of compositions, morphologies, and sizes.

Hollow carbon nanostructures

The fabrication of hollow carbon nanomaterials is of interest because of their outstanding properties and promising applications.[18–20,48–50] As expected, the RF resin coating strategy developed in this work can be extended as an effective route to produce hollow carbon nanomaterials with controllable structures. For instance, HCS were successfully obtained by the carbonization of the SiO_2@RF core–shell spheres followed by selective etching of SiO_2 by alkali. As illustrated in Fig. 4, the as-synthesized HCS preserve the structural integrity and spherical morphology. Based on the fact that the interior hollow size of HCS agrees well with the template SiO_2 spheres, the size of HCS can be precisely tunable by varying the size of the SiO_2 spheres. HCS with an interior hollow size of approximately 260 nm (designated as HCS-260) and 750 nm (designated as HCS-750) were synthesized by using SiO_2-260 and SiO_2-750 nm as the templates (Fig. 4).

The porosity of HCS was investigated by N_2 adsorption–desorption measurements (Fig. S5†). The N_2 sorption isotherms have clearly demonstrated the microporous porosity of the as-synthesized HCS-260. The BET surface area and the total pore volume of HCS-260 are 639.1 $m^2\ g^{-1}$ and 0.56 $cm^3\ g^{-1}$, respectively. It should be noted that the as-synthesized HCS with high specific surface area and large pore volume could have many applications in energy-storage media and electrode materials.[17,19] For instance, many reports suggested that carbon/sulfur composites are the most promising cathodes for lithium–sulfur batteries.[50,51] We demonstrate here that the cathodes based on HCS/sulfur composites have a potential application in lithium–sulfur batteries. By the convenient melt-diffusion strategy,[51] HCS-260/sulfur composites with ~70 wt% of sulfur content were obtained. At a current density of 500 mA g^{-1}, the initial capacity of HCS-260/sulfur composites was as high as 1260 mA h g^{-1}, which was ~75% of sulfur utilization based on the theoretical maximum 1675 mA h g^{-1} (Fig. S6†). The cell maintained a capacity of 740 mA h g^{-1} after 50 cycles, demonstrating that the synthetic strategy for HCS reported here could be helpful to explore and develop new electrode materials for lithium–sulfur batteries.

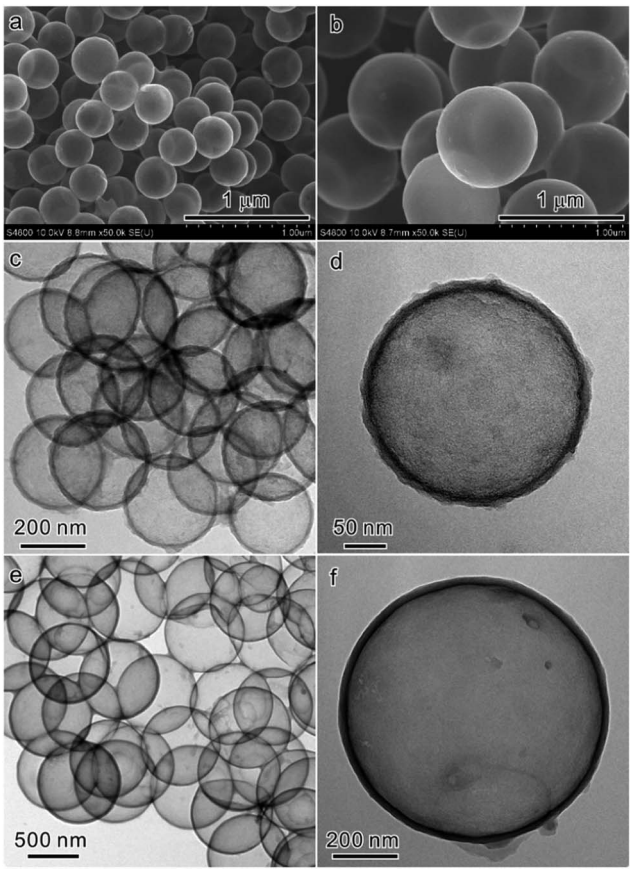

Fig. 4 SEM images: (a) HCS-260 and (b) HCS-750; TEM images: (c and d) HCS-260, and (e and f) HCS-750.

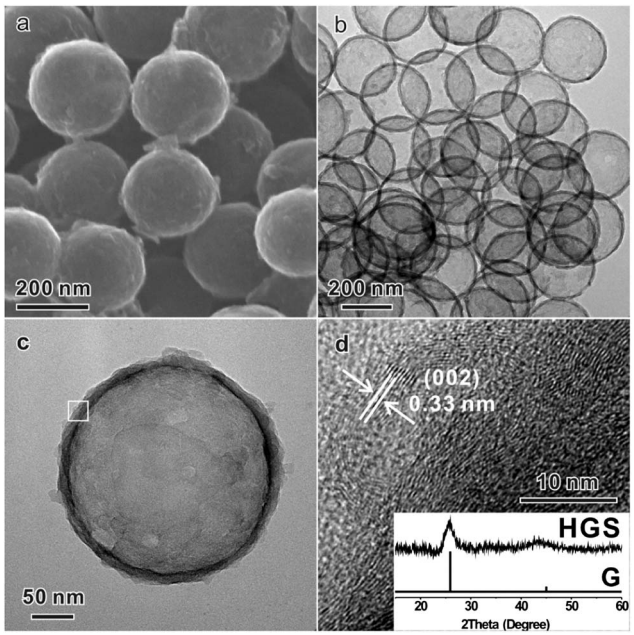

Fig. 5 (a) SEM image of HGS-260; (b and c) TEM images of HGS-260; (d) HRTEM image corresponding to the marked region in (c), inset: the XRD pattern of HGS-260 and simulated XRD pattern of graphite (designated as G).

Hollow graphitic nanostructures

Using the transition-metal species (*e.g.* Fe^{3+}, Co^{3+}, and Ni^{2+}) as the graphitization catalyst has recently been demonstrated as an effective route to synthesize graphitic carbon nanostructures from RF resin.[9,52] In order to demonstrate that our strategy could be further used to synthesize graphitic carbon nanostructures at low temperatures, carboxylic-functionalized SiO_2@RF core–shell spheres were synthesized simply by the addition of 4-dihydroxybenzoic acid to the same synthetic system. Fe^{3+} ions were then introduced into carboxylic-functionalized SiO_2@RF core–shell spheres.[53,54] After the carbonization of SiO_2@RF–Fe composites and subsequent removal of Fe species and SiO_2, HGS were obtained. Starting from SiO_2 spheres with a diameter of ~260 nm, as shown in Fig. 5a–c, HGS with an interior hollow size of ~260 nm (designated as HGS-260) were nicely synthesized. The high-resolution TEM images (Fig. 5d and S7†) reveal that the carbon shells of HGS-260 consist of graphitic carbon structures. The slight distortion of circular stripes could be attributed to defects formed during the graphitization process. The curved lattice fringes clearly show graphitic (002) layers with an interplanar spacing of 0.33 nm. The graphitized nature of HGS-260 was also confirmed by XRD analysis (inset of Fig. 5d). Due to the graphitized structure, the BET surface area of HGS-260 is smaller than HCS-260 (Fig. S5†). The BET surface area and total pore volume of HGS-260 are 396.8 $m^2\ g^{-1}$ and 0.51 $cm^3\ g^{-1}$, respectively.

To demonstrate the as-synthesized HGS as better support materials for catalysts, Pt nanoparticles were decorated onto the surface of HGS-260 and HCS-260 at a loading of 10 wt% Pt by the glycol-mediated reduction of K_2PtCl_6 (Fig. 6a).[9] For comparison, Pt nanoparticles were also deposited on a commercially available carbon support (*i.e.*, Vulcan-XC-72 carbon) using the same conditions. The TEM images (Fig. 6b–d) reveal that Pt nanoparticles with an average particle size of ~4 nm are successfully loaded onto the surface of HGS-260, HCS-260, and Vulcan-XC-72, respectively. The average crystallite sizes of Pt nanoparticles deduced from Scherrer's formula and from the XRD patterns of the as-synthesized Pt/HGS-260, Pt/HCS-260, and Pt/Vulcan-XC-72 (Fig. S8†) agree well with the evaluation results obtained from the TEM images. The size of the Pt nanoparticles on HGS-260, HCS-260, and Vulcan-XC-72 was similar. The as-synthesized Pt/HCS-260, Pt/HGS-260, and Pt/Vulcan-XC-72 were investigated for the electrocatalytic ORR in O_2-saturated 0.1 M $HClO_4$ solutions by using a rotating disk electrode (RDE) at room temperature. A characteristic set of polarization curves for the ORR on the as-synthesized Pt/HGS-260, Pt/HCS-260, and Pt/Vulcan-XC-72 are displayed in Fig. 6e. Two distinguishable potential regions are clearly observed in the polarization curves: the well-defined diffusion limiting current region below 0.6 V and the mixed kinetic-diffusion control region between 0.7 and 1.0 V. The ORR polarization curves show that the Pt/HGS-260 catalyst has more positive onset potentials than Pt/HCS-260 and Pt/Vulcan-XC-72 catalysts. In order to compare the activity of different catalysts, the kinetic currents (j_k) in the kinetic-diffusion control regions, which are normalized to the Pt mass,

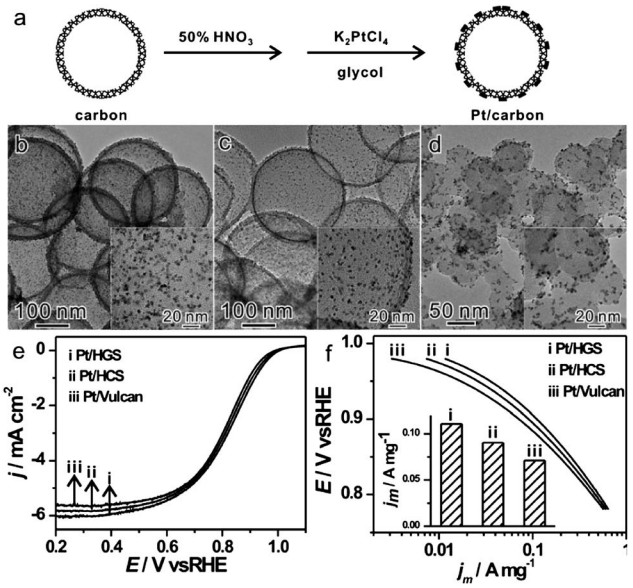

Fig. 6 (a) Scheme of the decoration of carbon supports by Pt nanoparticles; TEM images: (b) Pt/HGS-260, (c) Pt/HCS-260, and (d) Pt/Vulcan-XC-72 (inset: typical high-magnification TEM images); (e) ORR polarization curves for Pt/HGS-260, Pt/HCS-260, and Pt/Vulcan-XC-72 catalysts recorded at room temperature in an O_2-saturated 0.1 M $HClO_4$ aqueous solution at a sweep rate of 10 mV s^{-1} and a rotation rate of 1600 rpm. (f) Mass activity (j_{km}) for these three catalysts, which is given as kinetic current densities (j_k) normalized to the Pt mass. Insets show the activities at 0.9 V. The Pt loading of all catalysts modified on the RDEs is 15.3 μg cm^{-2}.

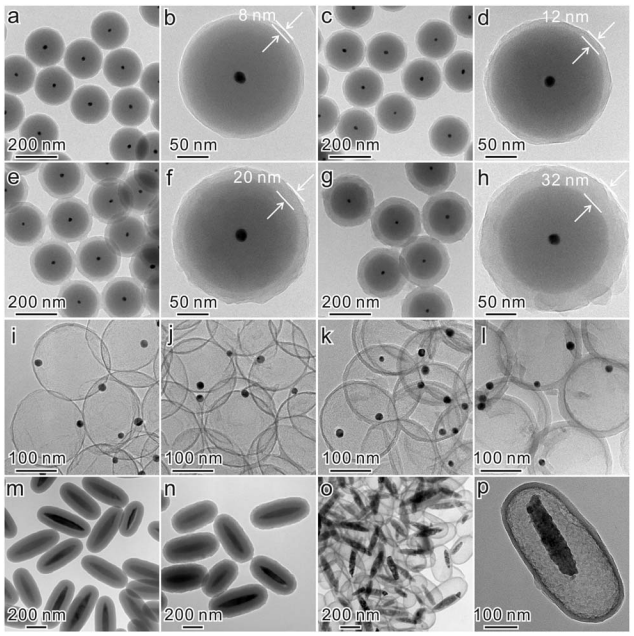

Fig. 7 TEM images: (a and b) Au@SiO_2@RF-I, (c and d) Au@SiO_2@RF-II, (e and f) Au@SiO_2@RF-III, (g and h) Au@SiO_2@RF-IV, (i) Au@HCS-I, (j) Au@HCS-II, (k) Au@HCS-III, (l) Au@HCS-IV, (m) α-Fe_2O_3@SiO_2, (n) α-Fe_2O_3@SiO_2@RF, (o and p) Fe_3O_4@HCS.

are calculated from the ORR polarization curves by using mass-transport correction (Fig. 6f). The Pt/HGS-260 catalyst exhibits a mass activity (j_{km}) of 0.11 A mg^{-1}, which is 1.2 and 1.6 times than that of Pt/HCS-260 (0.09 A mg^{-1}) and Pt/Vulcan-XC-72 (0.07 A mg^{-1}) catalysts, respectively. This result indicates the advantage of using HGS-260 and HCS-260 as a cathode catalyst support. The preferable performance of HGS-260 could be attributed to its unique graphitic structure although its surface area is smaller than that of HCS-260.[9–11]

Yolk–shell carbon nanostructures with ultrathin shells

The yolk–shell structures with catalytically active nanoparticles encapsulated in hollow porous shells have been recently demonstrated as an ideal nanoreactor framework to enhance the catalytic properties of the encapsulated nanoparticles.[55–59] Since the sol–gel derived SiO_2 has been widely used to fabricate SiO_2-coated composites,[8] the simple process for the synthesis of HCS can be extended as a general strategy to synthesize yolk–shell carbon nanostructures. More importantly, the precisely tailored RF resin coating reported here can provide an effective method to create yolk–shell carbon nanostructures with ultrathin shells, which is highly desired for carbon nanoreactors. For instance, when using Au@SiO_2 core–shell spheres (Fig. S9†) as templates, the sandwich-like Au@SiO_2@RF spheres with four different thicknesses of RF resin shells (denoted as Au@SiO_2@RF-I, -II, -III, and -IV, respectively) were readily obtained by regulating the ratio of Au@SiO_2 and RF resin precursors (Fig. 7a–h). The average thicknesses of RF resin shells of Au@SiO_2@RF-I, -II, -III, and -IV are about 8, 12, 20, and 32 nm, respectively. As shown in Fig. 7i–l, the corresponding Au@HCS yolk–shell nanoparticles (denoted as Au@HCS-I, -II, -III, and -IV, respectively) were obtained after carbonization and subsequent etching of SiO_2. The average thicknesses of carbon shells of Au@HCS-I, -II, -III, and -IV are about 3, 5, 9, and 13 nm, respectively. To the best of our knowledge, the Au@HCS-I within 3 nm ultrathin shells is the thinnest carbon shells compared with the previous carbon nanoreactors. In addition to spherical yolk–shell carbon nanostructures, nonspherical yolk–shell carbon nanostructures were also synthesized by using nonspherical SiO_2-coated composites as templates. As shown in Fig. 7m–p, ellipsoid-shaped Fe_3O_4@HCS yolk–shell nanoparticles were successfully prepared from ellipsoid-shaped α-Fe_2O_3@SiO_2 core–shell nanoparticles.

Owing to the structural feature that the functional core is isolated by a permeable carbon shell, one-in-one encapsulation of noble metal nanoparticles in HCS has been recognized as an effective route to improve their catalytic stability.[22–26] In order to demonstrate such a stabilizing effect in our yolk–shell carbon nanostructures, the reduction of 4-nitrophenol by $NaBH_4$ to 4-aminophenol was chosen as a model reaction to evaluate the catalytic ability and stability of the as-synthesized Au@HCS (Fig. 8a). The reduction process was monitored by UV-vis absorption spectroscopy of the reaction mixture (Fig. 8b and S10†). The reduction reaction did not proceed in the absence of Au@HCS catalysts, which was evidenced by a constant absorption peak at 410 nm. When Au@HCS catalysts were introduced into the solution, the characteristic absorption of 4-nitrophenol at 410 nm quickly decreased and the characteristic absorption of 4-aminophenol at 307 nm increased accordingly. The presence of two isosbestic points at 293 and 320 nm reveals that the

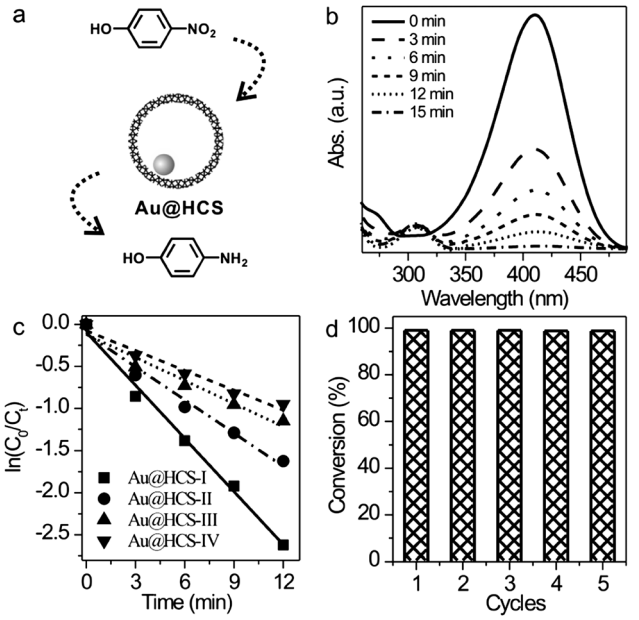

Fig. 8 (a) Schematic illustration: the reduction of 4-nitrophenol into 4-aminophenol by Au@HCS catalytic nanoreactors, (b) UV-vis spectra showing gradual reduction of 4-nitrophenol with Au@HCS-I, (c) plot of $\ln(C_t/C_0)$ *versus* time for Au@HCS-I, Au@HCS-II, Au@HCS-III, and Au@HCS-IV, respectively and (d) conversion of 4-nitrophenol in 5 successive cycles of reduction with Au@HCS-I.

reduction proceeded without producing byproducts. About 99% of 4-nitrophenol was converted into 4-aminophenol after 15 min reaction when using Au@HCS-I as the catalyst (Fig. 8b and S10†), clearly revealing that HCS in the as-synthesized Au@HCS are permeable to the reaction substances. For the same Au content of Au@HCS-II, -III, and -IV, conversions of 86%, 75%, and 70% were obtained within 15 min, respectively (Fig. S10†). A linear relationship of $\ln(C_t/C_0)$ *versus* time was observed for the Au@HCS catalysts (Fig. 8c), indicating that the reduction reaction can be considered as a pseudo-first-order reaction.[56] The rate constants of Au@HCS-I, -II, -III, and -IV are calculated to be -0.21 min^{-1}, -0.13 min^{-1}, -0.09 min^{-1}, and -0.08 min^{-1}, respectively. These results suggest that the thinner shell of nanoreactors facilitates the diffusion of the reactants and thus gives a much higher rate constant. The recyclability of Au@HCS for catalytic reduction of 4-nitrophenol was investigated to demonstrate the excellent stability of the present Au@HCS nanoreactors. As shown in Fig. 8d, even after 5 successive cycles of reactions, Au@HCS-I were still highly active with a conversion about 99% at 15 min. The high activity and stability of Au@HCS-I make the synthetic strategy developed in this work useful for the design of highly active and stable yolk–shell structured catalytic nanoreactors.

Conclusions

In summary, we have presented a facile approach to fabricate high-quality RF resin coated nanocomposites by CTAB assisted polymerization and deposition of RF resin on the surface of colloidal particles. This synthetic strategy is highly efficient and applicable to RF resin coated nanocomposites with different compositions, morphologies and sizes. The RF resin coating strategy developed in this work provided a versatile method for selective synthesis of core–shell, hollow, and yolk–shell carbon nanostructures. As the composition of RF resin shells can be adjusted simply by changing the reactant, graphitic carbon shells have successfully synthesized by the carboxylic functional RF resin coating strategy. The good capacity and cyclability of lithium–sulfur batteries by using HCS/sulfur composites, the preferable ORR performance of Pt/HGS, and high catalytic activity and stability of the Au@HCS nanoreactors with ultrathin shells demonstrate that the proposed RF resin coating strategy is a powerful platform for the synthesis and applications of hollow and yolk–shell carbon nanostructures. The synthesis of the RF resin coated nanocomposites in this work can be exploited to design functional carbon nanomaterials for other research fields, such as lithium batteries, supercapacitor electrodes, and environmental protection.

Acknowledgements

We thank the MOST of China (2011CB932403, 2009CB930703), the NSFC (21131005, 21021061, 20925103, 20923004), and the Fok Ying Tung Education Foundation (121011) for the financial support.

Notes and references

1 X. W. Lou, L. A. Archer and Z. Yang, *Adv. Mater.*, 2008, **20**, 3987.
2 K. An and T. Hyeon, *Nano Today*, 2009, **4**, 359.
3 Q. Zhang, W. Wang, J. Goebl and Y. Yin, *Nano Today*, 2009, **4**, 494.
4 P. Reiss, M. Protiere and L. Li, *Small*, 2009, **5**, 154.
5 Y. Zhao and L. Jiang, *Adv. Mater.*, 2009, **21**, 3621.
6 G. L. Li, H. Möhwald and D. G. Shchukin, *Chem. Soc. Rev.*, 2013, **42**, 3628.
7 X. L. Fang, C. Chen, Z. H. Liu, P. X. Liu and N. F. Zheng, *Nanoscale*, 2011, **3**, 1632.
8 X. L. Fang, X. J. Zhao, W. J. Fang, C. Chen and N. F. Zheng, *Nanoscale*, 2013, **5**, 2205.
9 Z. L. Schaefer, M. L. Gross, M. A. Hickner and R. E. Schaak, *Angew. Chem., Int. Ed.*, 2010, **49**, 7045.
10 B. Y. Xia, J. N. Wang, X. X. Wang, J. J. Niu, Z. M. Sheng, M. R. Hu and Q. C. Yu, *Adv. Funct. Mater.*, 2008, **18**, 1790.
11 Z. M. Sheng and J. N. Wang, *Adv. Mater.*, 2008, **20**, 1071.
12 S. Shanmugam and A. Gedanken, *Small*, 2007, **3**, 1189.
13 W. M. Zhang, X. L. Wu, J. S. Hu, Y. G. Guo and L. J. Wan, *Adv. Funct. Mater.*, 2008, **18**, 3941.
14 X. W. Lou, C. M. Li and L. A. Archer, *Adv. Mater.*, 2009, **21**, 2536.
15 S. H. Ng, J. Wang, D. Wexler, K. Konstantinov, Z. P. Guo and H. K. Liu, *Angew. Chem., Int. Ed.*, 2006, **45**, 6896.
16 S. Yang, X. Feng, L. Zhi, Q. Cao, J. Maier and K. Müllen, *Adv. Mater.*, 2010, **22**, 838.
17 N. Jayaprakash, J. Shen, S. S. Moganty, A. Corona and L. A. Archer, *Angew. Chem., Int. Ed.*, 2011, **50**, 5904.

18 G. S. Chai, S. B. Yoon, J. H. Kim and J. S. Yu, *Chem. Commun.*, 2004, 2766.
19 K. Xie, X. Qin, X. Wang, Y. Wang, H. Tao, Q. Wu, L. Yang and Z. Hu, *Adv. Mater.*, 2012, **24**, 347.
20 L. M. Guo, L. X. Zhang, J. M. Zhang, J. Zhou, Q. J. He, S. Z. Zeng, X. Z. Cui and J. L. Shi, *Chem. Commun.*, 2009, 6071.
21 W. S. Seo, J. H. Lee, X. Sun, Y. Suzuki, D. Mann, Z. Liu, M. Terashima, P. C. Yang, M. V. McConnell, D. G. Nishimura and H. Dai, *Nat. Mater.*, 2006, **5**, 971.
22 M. Kim, K. Sohn, H. Bin Na and T. Hyeon, *Nano Lett.*, 2002, **2**, 1383.
23 S. Ikeda, S. Ishino, T. Harada, N. Okamoto, T. Sakata, H. Mori, S. Kuwabata, T. Torimoto and M. Matsumura, *Angew. Chem., Int. Ed.*, 2006, **45**, 7063.
24 T. Harada, S. Ikeda, Y. H. Ng, T. Sakata, H. Mori, T. Torimoto and M. Matsumura, *Adv. Funct. Mater.*, 2008, **18**, 2190.
25 Y. H. Ng, S. Ikeda, T. Harada, S. Higashida, T. Sakata, H. Mori and M. Matsumura, *Adv. Mater.*, 2007, **19**, 597.
26 T. Harada, S. Ikeda, F. Hashimoto, T. Sakata, K. Ikeue, T. Torimoto and M. Matsumura, *Langmuir*, 2010, **26**, 17720.
27 A. H. Lu, T. Sun, W. C. Li, Q. Sun, F. Han, D. H. Liu and Y. Guo, *Angew. Chem., Int. Ed.*, 2011, **50**, 11765.
28 Y. Zhai, Y. Dou, D. Zhao, P. F. Fulvio, R. T. Mayes and S. Dai, *Adv. Mater.*, 2011, **23**, 4828.
29 X. Sun and Y. Li, *Angew. Chem., Int. Ed.*, 2004, **43**, 597.
30 R. J. White, K. Tauer, M. Antonietti and M. M. Titirici, *J. Am. Chem. Soc.*, 2010, **132**, 17360.
31 B. Hu, K. Wang, L. Wu, S. H. Yu, M. Antonietti and M. M. Titirici, *Adv. Mater.*, 2010, **22**, 813.
32 S. Ikeda, K. Tachi, Y. H. Ng, Y. Ikoma, T. Sakata, H. Mori, T. Harada and M. Matsumura, *Chem. Mater.*, 2007, **19**, 4335.
33 H. Lee, S. M. Dellatore, W. M. Miller and P. B. Messersmith, *Science*, 2007, **318**, 426.
34 A. Postma, Y. Yan, Y. J. Wang, A. N. Zelikin, E. Tjipto and F. Caruso, *Chem. Mater.*, 2009, **21**, 3042.
35 H. Jiang, L. Yang, C. Li, C. Yan, P. S. Lee and J. Ma, *Energy Environ. Sci.*, 2011, **4**, 1813.
36 R. Liu, S. M. Mahurin, C. Li, R. R. Unocic, J. C. Idrobo, H. Gao, S. J. Pennycook and S. Dai, *Angew. Chem., Int. Ed.*, 2011, **50**, 6799.
37 S. A. Al-Muhtaseb and J. A. Ritter, *Adv. Mater.*, 2003, **15**, 101.
38 A. M. Elkhatat and S. A. Al-Muhtaseb, *Adv. Mater.*, 2011, **23**, 2887.
39 J. Lee, J. Kim and T. Hyeon, *Adv. Mater.*, 2006, **18**, 2073.
40 C. Liang, Z. Li and S. Dai, *Angew. Chem., Int. Ed.*, 2008, **47**, 3696.
41 A. H. Lu and F. Schüth, *Adv. Mater.*, 2006, **18**, 1793.
42 J. Liu, S. Z. Qiao, H. Liu, J. Chen, A. Orpe, D. Zhao and G. Q. Lu, *Angew. Chem., Int. Ed.*, 2011, **50**, 5947.
43 S. Wang, W. C. Li, G. P. Hao, Y. Hao, Q. Sun, X. Q. Zhang and A. H. Lu, *J. Am. Chem. Soc.*, 2011, **133**, 15304.
44 D. Fujikawa, M. Uota, G. Sakai and T. Kijima, *Carbon*, 2007, **45**, 1289.
45 Y. Dai, B. Lim, Y. Yang, C. M. Cobley, W. Li, E. C. Cho, B. Grayson, P. T. Fanson, C. T. Campbell, Y. Sun and Y. Xia, *Angew. Chem., Int. Ed.*, 2010, **49**, 8165.
46 Z. Chen, Z. M. Cui, F. Niu, L. Jiang and W. G. Song, *Chem. Commun.*, 2010, **46**, 6524.
47 H. Bao, J. Yang, Y. Huang, Z. P. Xu, N. Hao, Z. Wu, G. Q. Lu and D. Zhao, *Nanoscale*, 2011, **3**, 4069.
48 Q. Sun, W. C. Li and A. H. Lu, *Small*, 2013, DOI: 10.1002/smll.201202671.
49 Z. A. Qiao, B. Guo, A. J. Binder, J. Chen, G. M. Veith and S. Dai, *Nano Lett.*, 2012, **13**, 207.
50 G. Zheng, Y. Yang, J. J. Cha, S. S. Hong and Y. Cui, *Nano Lett.*, 2011, **11**, 4462.
51 X. Ji, K. T. Lee and L. F. Nazar, *Nat. Mater.*, 2009, **8**, 500.
52 S. J. Han, Y. K. Yun, K. W. Park, Y. E. Sung and T. Hyeon, *Adv. Mater.*, 2003, **15**, 1922.
53 A. H. Lu, W. C. Li, G. P. Hao, B. Spliethoff, H. J. Bongard, B. B. Schaack and F. Schüth, *Angew. Chem., Int. Ed.*, 2010, **49**, 1615.
54 G. H. Wang, Q. Sun, R. Zhang, W. C. Li, X.-Q. Zhang and A. H. Lu, *Chem. Mater.*, 2011, **23**, 4537.
55 P. M. Arnal, M. Comotti and F. Schüth, *Angew. Chem., Int. Ed.*, 2006, **45**, 8224.
56 J. Lee, J. C. Park and H. Song, *Adv. Mater.*, 2008, **20**, 1523.
57 X. Q. Huang, C. Y. Guo, J. Q. Zuo, N. F. Zheng and G. D. Stucky, *Small*, 2009, **5**, 361.
58 X. L. Fang, Z. H. Liu, M. F. Hsieh, M. Chen, P. X. Liu, C. Chen and N. F. Zheng, *ACS Nano*, 2012, **6**, 4434.
59 Z. H. Liu, X. L. Fang, C. Chen and N. F. Zheng, *Acta Chim. Sin.*, 2013, **71**, 334.